Neural network interatomic potential for the phase change material GeTe

Gabriele C. Sosso,[1] Giacomo Miceli,[1,*] Sebastiano Caravati,[2] Jörg Behler,[3] and Marco Bernasconi[1,†]

[1]*Dipartimento di Scienza dei Materiali, Università di Milano-Bicocca, Via R. Cozzi 53, I-20125 Milano, Italy*

[2]*Department of Chemistry and Applied Biosciences, ETH Zurich, and Facoltà di Informatica, Istituto di Scienze Computazionali, Università della Svizzera Italiana, Via Giuseppe Buffi 13, 6900 Lugano, Switzerland*

[3]*Lehrstuhl für Theoretische Chemie, Ruhr-Universität Bochum, D-44780 Bochum, Germany*

(Received 12 January 2012; published 4 May 2012)

GeTe is a prototypical phase change material of high interest for applications in optical and electronic nonvolatile memories. We present an interatomic potential for the bulk phases of GeTe, which is created using a neural network (NN) representation of the potential-energy surface obtained from reference calculations based on density functional theory. It is demonstrated that the NN potential provides a close to *ab initio* quality description of a number of properties of liquid, crystalline, and amorphous GeTe. The availability of a reliable classical potential allows addressing a number of issues of interest for the technological applications of phase change materials, which are presently beyond the capability of first-principles molecular dynamics simulations.

DOI: 10.1103/PhysRevB.85.174103 PACS number(s): 31.50.Bc, 31.15.xv

I. INTRODUCTION

Phase change materials based on chalcogenide alloys are attracting an increasing interest worldwide due to their ability to undergo reversible and fast transitions between the amorphous and crystalline phases upon heating.[1] This property is exploited in rewritable optical media (CD, DVD, Blu-Ray Discs) and electronic nonvolatile memories (NVM), which are based on the strong optical and electronic contrast between the two phases.[2,3] The material of choice for NVM applications is the ternary compound $Ge_2Sb_2Te_5$ (GST). However, the related binary alloy GeTe has also been thoroughly investigated because of its higher crystallization temperature and better data retention at high temperature with respect to GST.

In the last few years, atomistic simulations based on density functional theory (DFT) have provided useful insights into the properties of phase change materials.[4–9] However, several key issues such as the thermal conductivity at the nanoscale and the properties of the crystalline/amorphous interface or of nanowires, just to name a few, are presently beyond the reach of *ab initio* simulations due to the high computational costs. The development of reliable classical interatomic potentials is a possible route to overcome the limitations in system size and time scale of *ab initio* molecular dynamics. However, traditional approaches based on the fitting of simple functional forms for the interatomic potentials are very challenging due to the complexity of the chemical bonding in the crystalline and amorphous phases revealed by the *ab initio* simulations. A possible solution has been proposed recently by Behler and Parrinello,[10] who developed high-dimensional interatomic potentials with close to *ab initio* accuracy employing artificial neural networks (NN). To date, potentials of this type have been reported for silicon,[11,12] carbon,[13,14] sodium,[15] zinc oxide,[16] and copper[17] by fitting large *ab initio* databases.

Here, we describe the development of a classical interatomic potential for the bulk phases of GeTe employing this NN technique. The potential is validated by comparing results on the structural and dynamical properties of liquid, amorphous, and crystalline GeTe derived from NN-based simulations with the *ab initio* data obtained here and in our previous work.[18]

II. METHODS

A. Neural network method

Artificial neural networks constitute a class of algorithms inspired by the properties of biological neural networks, which are widely applied in many different fields ranging from weather forecasting to robotics.[19] In the last few years, NN have also been used as a tool to construct interatomic potentials.[20,21] To this aim, the NN are exploited as a nonlinear technique that allows fitting any real-valued function to arbitrary accuracy, without any previous knowledge about the functional form of the underlying problem.[22,23] In our case, this function is the potential energy surface (PES) of the atomistic system and the goal of the NN is to construct a functional relation between the energy and the atomic configuration.

Given a number of atomic configurations, for which the *ab initio* energies are known, the NN parameters are adjusted to reproduce these energies in the training process. Overfitting, i.e., obtaining a good fit of the training data, but performing less accurately when making predictions, is controlled by testing the performance of the NN for an independent test set not used in the fitting. Once trained, the NN performs an interpolation to construct the potential energy for new atomic configurations at a low computational load, which allows performing long molecular dynamics runs for large systems.

The NN methodology overcomes many problems associated with classical potentials. First and foremost, NN completely obviate the problem of guessing a complicated functional form of the interatomic potential. This form is determined automatically by the NN. Moreover, the entire training procedure is fully automated so that NN can be readily extended to new regions of the PES. Finally, the accurate mapping of *ab initio* energies ensures that all properties determined by the topology of the PES are described with an accuracy comparable with that of first-principles calculations. NN have been successfully used to interpolate the PES of simple chemical systems such as small molecules[24–28] and molecule-surface interactions.[29–34]

Until recently, the main limitation of most NN approaches has been the small number of degrees of freedom that could

be described, which confined their application to very small systems. This limitation has been overcome by Behler and Parrinello who introduced a NN potential, in which the total energy is expressed as a sum of atomic energy contributions depending on the local environments.[10] In this approach, the energy contribution of each atom is evaluated using an individual NN instead of using one NN for the total energy of the system. The local environment of a given atom is described by a set of local parameters called symmetry functions, which include radial and angular many-body terms and depend on the positions of all neighbors within a specified cutoff radius.[35] The use of symmetry functions instead of Cartesian coordinates as NN inputs and the partitioning of the total energy into atomic contributions ensures that all quantities computed with the NN potential, such as energies, analytical forces, and stress tensor are invariant to translations, rotations, and atoms exchange. Furthermore, once the fit is obtained, the NN potential can be applied to systems containing an arbitrary number of atoms. The validity of this approach has been demonstrated by reproducing the high-pressure phase diagram of silicon, carbon, and sodium.[11,13,15] This scheme has been recently extended to binary systems by including long-range Coulomb interaction between environment-dependent ionic charges.[16,36]

In the case of GeTe, we are faced with the problem of developing a potential suitable to describe both the semiconducting crystalline and amorphous phases as well as the metallic liquid. As a first step toward the development of a NN potential for GeTe, we neglect long-range Coulomb interactions for atoms being separated by a larger distance than the cutoff radius of the symmetry functions. The resulting "short-ranged" NN potential just consists of atomic energy contributions arising from the local chemical environments, but it is important to note that also short-ranged electrostatic interactions are fully taken into account implicitly. More details of the employed method can be found elsewhere.[10,35] The resulting potential will not be able to describe the dielectric response and longitudinal optical– transverse optical (LO–TO) splitting of crystalline GeTe in its ferroelectric phase, but it will be suitable to reproduce structural properties of the liquid, amorphous, and crystalline phases and the dynamical properties of the disordered phases.

B. NN potential for GeTe

To generate the NN potential, we fitted the total energies of about 30 000 configurations of 64-, 96-, and 216-atom supercells computed within density functional theory (DFT). We started with a relatively small dataset of about 5000 structures, where we considered crystalline configurations, snapshots of the liquid phase and of the amorphous phase generated by quenching from the melt at ambient conditions and at different pressures up to 50 GPa. We also considered mixed crystalline/amorphous models generated by partially crystallizing the amorphous phase by means of the metadynamics technique.[37] All these configurations were generated within DFT molecular dynamics simulations at different temperatures (up to 3000 K) with the code CP2K (Ref. 38) and the Perdew-Burke-Ernzerhof (PBE) (Ref. 39) exchange-correlation functional. The Kohn-Sham orbitals were expanded in a triple-zeta-valence plus polarization (TZVP) Gaussian-type basis set, and the charge density was expanded in a plane-wave basis set with a cutoff of 100 Ry to efficiently solve the Poisson equation within the QUICKSTEP scheme.[38] Goedecker-type pseudopotentials[40] with four and six valence electrons were used for Ge and Te, respectively. Brillouin zone (BZ) integration was restricted to the supercell Γ point. A time step of 2 fs was used for the simulations. The same scheme was applied in our previous works on GeTe, GST, and other phase change materials[6,7,41,42] and previously validated by comparison with plane-wave molecular dynamics simulations with the CPMD code.[58] This framework was used to generate the atomic configurations for the fitting of the NN potential and to generate the DFT models of liquid and amorphous GeTe to check to transferability of the NN potential. However, since the NN fitting relies only on tiny differences in the total energy of supercells also including configurations with different number of atoms, a very high accuracy in the total energy is mandatory. An accurate integration of the BZ is indeed needed to achieve the required convergence in the total energy for the NN fitting. To generate the energies dataset for the fitting, we thus used the atomic configurations generated with the CP2K code and computed their total energy by performing BZ integration over a dense $4 \times 4 \times 4$ Monkhorst-Pack[43] (MP) mesh for the 64-atom cell and employing meshes of a corresponding k-point density for the larger systems. To this aim, we used the QUANTUM-ESPRESSO package.[44] Norm-conserving pseudopotentials were employed, considering only the outermost s and p electrons in the valence shell. The Kohn-Sham orbitals were expanded in a plane-wave basis up to a kinetic energy cutoff of 40 Ry. These settings ensure convergence of the total energy to 2 meV/atom. The fact that we used two different DFT setups to generate the atomic configurations and to compute their total energy for the NN fitting is immaterial as we could have generated the atomic configurations by any means including empirical interatomic potentials provided that the database is large enough to include all the relevant configurations.

This first dataset was then expanded by adding randomly distorted structures of the initial dataset at slightly different pressures and temperatures and models with slight deviations from the perfect stoichiometry. The refinement of the potential was achieved by inserting in the data set the *ab initio* energy of configurations generated by molecular dynamics simulations (see below) using the not yet refined NN potential.

The best NN fit we found employs three hidden layers with 20 nodes each. Sigmoidal activation functions were used in the nodes of the hidden layers, while a linear function was used for the output node. Details concerning the architecture of the NN can be found elsewhere.[35] The local environment of each atom is defined by the value of 159 symmetry functions (see Ref. 35 for details) defined in terms of the positions of all neighbors within a distance cutoff of 6.88 Å. We checked that by decreasing the cutoff from 6.88 to 6.00 Å, the structural properties of the liquid and amorphous phases do not change by inspection on the partial pair correlation functions. However, the larger cutoff turned out to be necessary to reproduce the DFT diffusion coefficient of the liquid. The generation of the NN potential and the calculation of the forces for the MD simulations were performed with the NN code

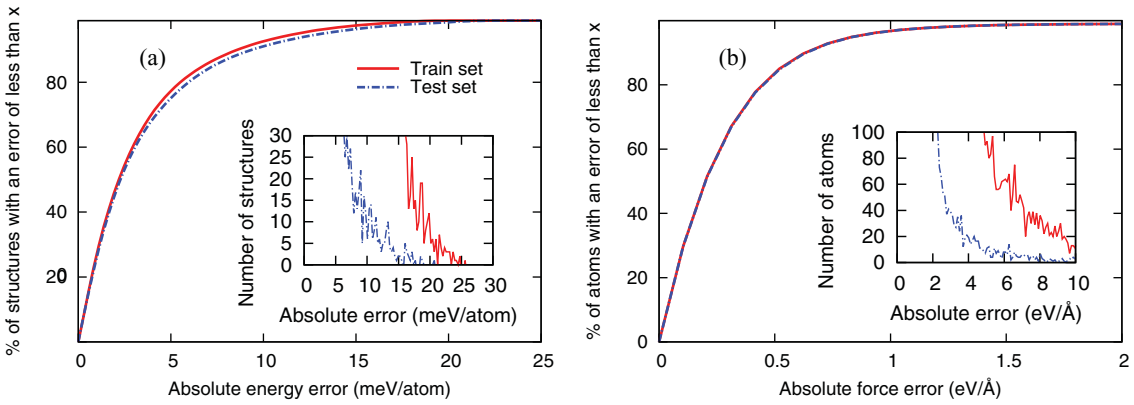

FIG. 1. (Color online) Normalized cumulative histograms of the absolute NN errors in training and test data sets for the energies (a) and forces (b). Standard histograms for the same data are presented as insets.

RUNNER.[45] We used the TINKER (Ref. 46) code as MD driver. The time step for the MD runs was set to 0.2 fs, and constant temperature simulations were performed using the Berendsen thermostat.[47]

The results of the fitting process of the NN potential are summarized in Fig. 1. The root-mean-square error (RMSE) for the energy is 5.01 and 5.60 meV/atom for the training and the test set, respectively, while the RMSEs of the forces are 0.46 and 0.47 eV/Å for the two sets. Among all structures considered, only a negligible fraction shows noticeable absolute errors, up to 25.8 meV/atom and 11.2 eV/Å for energies and forces (see Fig. 1 insets). We have found that these configurations correspond to high-energy structures that are not visited in MD simulations carried out in this work.

III. RESULTS

A. Crystalline phase

The equilibrium geometry of the trigonal phase of crystalline GeTe ($R3m$ space group) was obtained by optimizing all structural parameters consisting of the lattice parameter a, the trigonal angle α, and the internal parameter x that assigns the positions of the two atoms in the unit cell, namely, Ge at (x,x,x) and Te at $(-x,-x,-x)$.[48] The residual anisotropy in the stress tensor at the optimized lattice parameter at each volume is below 0.02 kbar. The energy versus volume data were fitted with a Murnaghan equation of state.[49] The theoretical structural parameters of the trigonal phase of GeTe at equilibrium are compared in Table I with experimental data[48] and DFT results obtained with a $12 \times 12 \times 12$ MP k-point mesh in the BZ integration. DFT data are similar to those reported previously.[50] The lengths of the short and long Ge-Te bonds are also given. The structure of trigonal GeTe can be seen as a distorted rocksalt geometry with an elongation of the cube diagonal along the [111] direction and an off-center displacement of the inner Te atom along the [111] direction, which moves to a distance d from the Ge atom at the vertex as shown in Fig. 2(a). The energy gained by the off-center displacement is analyzed by varying the distance

TABLE I. Structural parameters of the trigonal phase of crystalline GeTe from NN and DFT calculations and from the experimental data of Ref. 48. The lengths of the short and long bonds are also given.

Structural parameters	NN	DFT	Expt.
a (Å)	4.47	4.33	4.31
α	55.07°	58.14°	57.9°
Volume (Å^3)	55.95	54.98	53.88
x	0.2324	0.2358	0.2366
Short, long bonds (Å)	2.81, 3.31	2.85, 3.21	2.84, 3.17

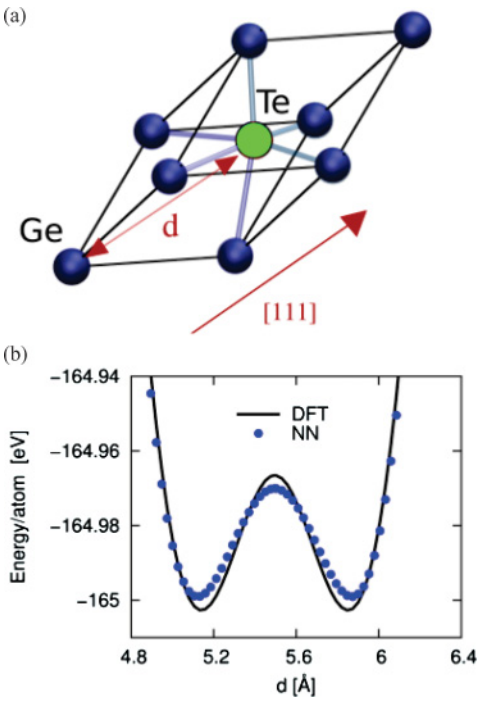

FIG. 2. (Color online) (a) Trigonal structure of crystalline GeTe, which can be seen as a cubic rocksalt geometry with an elongation of the [111] diagonal. Ge atoms are on the vertexes of the cell, while Te atom stands in the center. The distance between Ge and Te atoms along the [111] direction is indicated by d. (b) Energy of trigonal GeTe as a function of d at fixed values of the lattice parameters at the theoretical equilibrium geometry (cf. Table I).

TABLE II. Elastic constants (GPa) of trigonal GeTe from DFT and NN calculations.

	c_{11}	c_{12}	c_{13}	c_{14}	c_{33}	c_{44}
DFT	92	18	22	35	40	24
NN	73	10	30	24	36	20

d at fixed lattice parameters a and α. The resulting energy as a function of d is reported in Fig. 2(b) for the NN and the DFT calculations. We note that the DFT values in Fig. 2 were not included in the training set but were recalculated for investigating the quality of the NN potential only. The double-well potential identifies the two possible ferroelectric configurations, while the maximum corresponds to an ideal paraelectric configuration.

As a further validation of the potential, we computed the difference in energy between the trigonal phase and an ideal rocksalt phase at their equilibrium volumes at zero temperature that amounts to 44 or 55 meV/atom in NN and DFT calculations, respectively.

The elastic properties of trigonal GeTe were investigated by computing the elastic constants from finite deformations of the lattice parameters. The NN and DFT results are compared in Table II. The elastic constants obtained here with the PBE functional are somehow softer than those obtained with the LDA functional in Ref. 51. The bulk modulus obtained either from the elastic constants or from the equation of state is 34 and 36 GPa for the NN and DFT calculations.

The agreement between NN and DFT results is overall very good, the largest discrepancy being the cell angle and the difference between the short and long Ge-Te bonds, which might also be the source of the slight misfit in the elastic constants. The results are overall satisfactory considering that long-range Coulomb interactions are not included in our NN potential for the reasons discussed in Sec. II A. These are expected to play a role in the ferroelectric crystalline phase of GeTe, but they are probably less important in the liquid and amorphous phases we are primarily interested in.

B. Liquid phase

The liquid phase of GeTe was simulated by a 4096-atom model at 1150 K. Total and partial pair correlation functions are compared in Fig. 3 with results from our previous *ab initio* simulations in a small 216-atom cell at the same temperature.[18] Results from the NN simulations of a 216-atom cell are also reported. The density of 0.03156 atoms/Å^3 is the same for all simulations and corresponds to the value chosen in the *ab initio* simulations of Ref. 18, which is close to the experimental density of the amorphous phase.[52] Distributions of coordination numbers are reported in Fig. 4 as computed by integrating the partial pair correlation functions up to the cutoff shown in Fig. 3. Average coordination numbers are

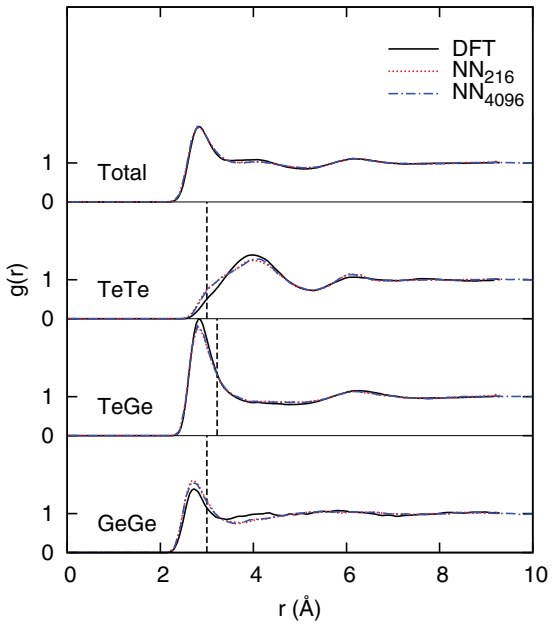

FIG. 3. (Color online) Total and partial pair correlation functions of liquid GeTe from a NN molecular dynamics simulation at 1150 K with a 4096- and a 216-atom cell, compared with results from a DFT simulation at the same temperature using a 216-atom cell (Ref. 18). NN results are obtained by averaging over a NVE run 40 ps long at the average temperature of 1150 K. The vertical lines are the interatomic distance threshold used to define the coordination numbers 3.0, 3.22, and 3.0 Å for Ge-Ge, Ge-Te, and Te-Te bonds, respectively.

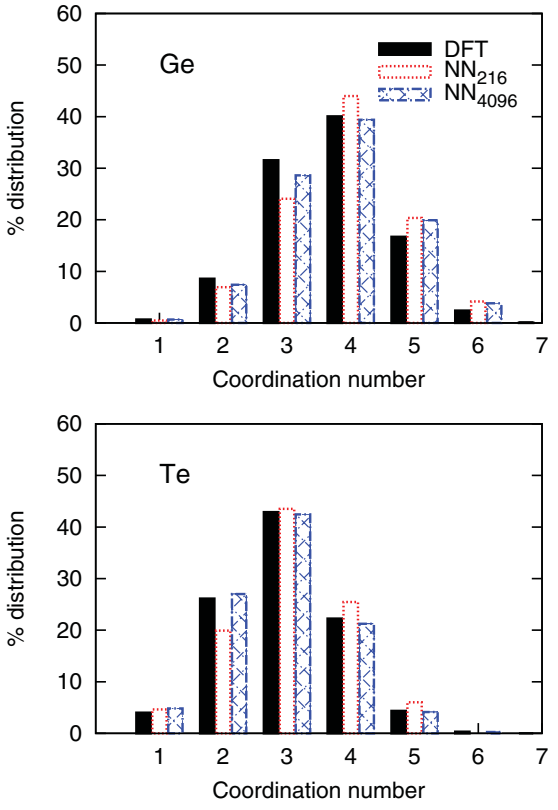

FIG. 4. (Color online) Distributions of coordination numbers of Ge and Te atoms in liquid GeTe at 1150 K. Results from NN (4096- and 216-atom) and DFT (216-atom) (Ref. 18) simulations are compared.

TABLE III. Average coordination numbers for different pairs of atoms computed from the partial pair correlation functions of liquid GeTe from a NN molecular dynamics simulation at 1150 K with a 4096- and a 216-atom cell (cf. Fig. 3), compared with results from a DFT simulation of a 216-atom cell at the same temperature (Ref. 18). The interatomic distance thresholds defined in Fig. 3 are used.

	With Ge			With Te			Total		
	DFT	NN_{216}	NN_{4096}	DFT	NN_{216}	NN_{4096}	DFT	NN_{216}	NN_{4096}
Ge	1.00	1.11	1.15	2.71	2.78	2.67	3.71	3.89	3.82
Te	2.71	2.78	2.67	0.26	0.28	0.26	2.97	3.07	2.93

given in Table III, while angle distribution functions are shown in Fig. 5. The agreement between NN and *ab initio* data is excellent. The NN results obtained with 216- and 4096-atom cells are extremely similar, which demonstrates that structural properties of the liquid can be reliably described by the cells few hundred atoms large we used in our previous *ab initio* works.[6,7,18,41,42] The self-diffusion coefficients computed from NN simulations are also in good agreement with the *ab initio* results of Ref. 8 as shown in Table IV. These latter data refer to simulations at 1000 K to enable a comparison with previous *ab initio* results obtained at this temperature.

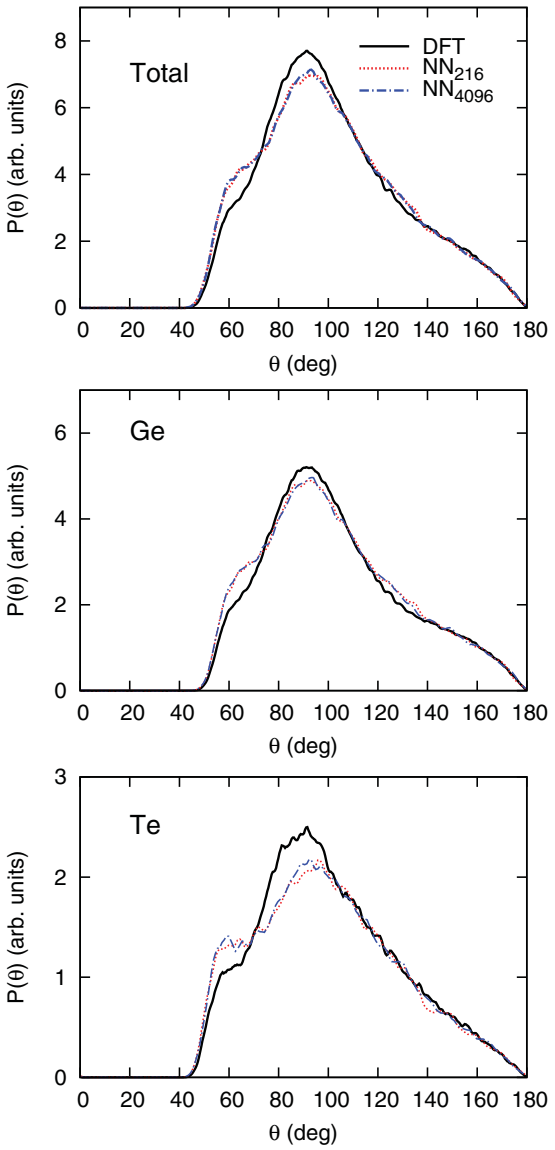

FIG. 5. (Color online) Total and partial angle distribution functions of liquid GeTe from a NN molecular dynamics simulation at 1150 K with a 4096- and a 216-atom cell, compared with results from a DFT simulation at the same temperature using a 216-atom cell (Ref. 18). Partial distributions refer to X-Ge-Y and X-Te-Y triplets (X,Y = Ge or Te).

C. Amorphous phase

The structural properties of a-GeTe and a-GST have been elucidated recently by *ab initio* simulations.[6–9,18,53] In these systems, Ge and Te atoms are mostly four-coordinated and three-coordinated, respectively. Te atoms are in a defective octahedral-like environment, which resembles the local environment of the corresponding crystalline phases. The majority of Ge atoms are in a defective octahedral environment too, but about one quarter of Ge atoms are in a tetrahedral-like geometry. The presence of homopolar Ge-Ge (and, in the case of GST, Ge-Sb) bonds favors the tetrahedral coordination.

In the following, we compare the structural properties of models of amorphous GeTe generated by NN and DFT simulations. The DFT simulations were performed with the CP2K code and the framework described in Sec. II B. A large NN amorphous model was generated by quenching the 4096-atom liquid model. We also considered 10 small 216-atom NN models of a-GeTe to investigate the size of the fluctuations in the structural properties due to the use of a small cell. For sake of comparison, we similarly generated 10 216-atom DFT models of a-GeTe by quenching the melt in 100 ps at the same density of 0.03156 atoms/Å^3. The NN amorphous models were generated by quenching the molten sample from 1150 K to room temperature in 100 ps. Average properties are obtained from a NVE simulation 40 ps long at an average temperature of 300 K. Doubling or even tripling

TABLE IV. Diffusion coefficient of Ge and Te atoms in the 4096-atom model of liquid GeTe at 1000 K. NN results were obtained from the slope of the mean-square displacement versus time. The same values within the figures given here are obtained from the integral of the velocity-velocity autocorrelation function. DFT data of a 216-atom cell at the same temperature are from Ref. 8.

	NN	DFT
D_{Ge} (10^{-5} cm^2/s)	4.96	4.65
D_{Te} (10^{-5} cm^2/s)	3.62	3.93

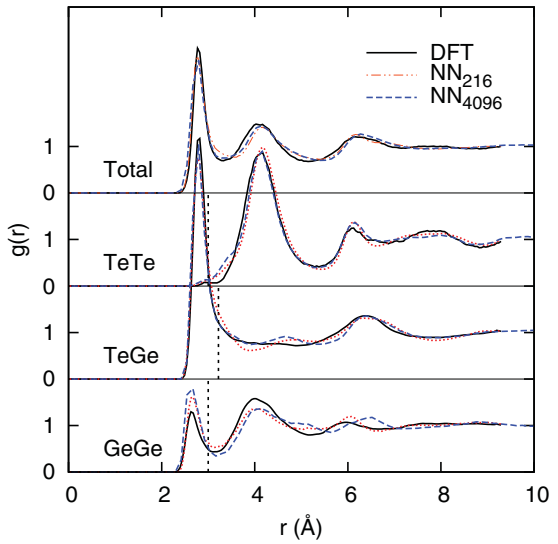

FIG. 6. (Color online) Total and partial pair correlation functions of amorphous GeTe from a NN molecular dynamics simulation at 300 K with a 4096- and 216-atom cell, compared with results from DFT simulation at the same temperature using 216-atom cells. The vertical lines are the interatomic distance thresholds used to define the coordination numbers 3.0, 3.22, and 3.0 Å for Ge-Ge, Ge-Te, and Te-Te bonds, respectively. NN and DFT data for the small cell are averaged over 10 independent models here and in all the subsequent figures if not specified otherwise.

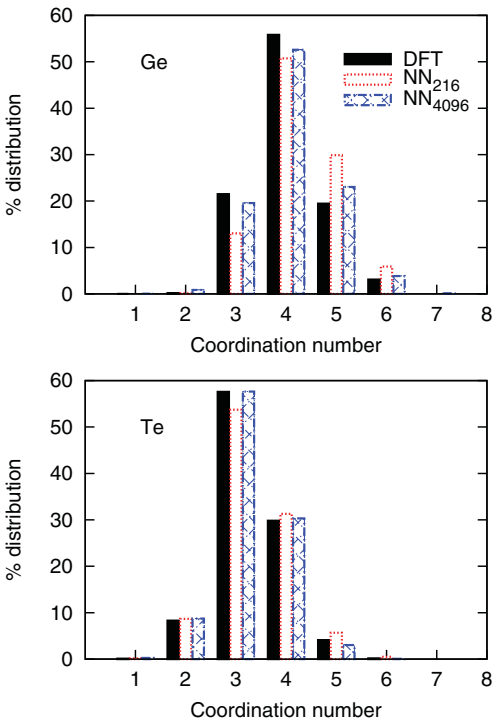

FIG. 7. (Color online) Distribution of coordination numbers of Ge and Te atoms in a-GeTe from NN and DFT simulations with 4096- and 216-atom cells. The interatomic distance thresholds defined in Fig. 6 are used.

the quenching time (up to 300 ps) does not introduce sizable changes in the structural and vibrational properties of our NN 4096-atom model of a-GeTe. Structural properties are described in Figs. 6–9. The partial pair correlation functions of our NN models are compared with DFT data in Fig. 6. The distribution of coordination numbers and their average values are reported in Fig. 7 and Table V for NN and DFT simulations. Bond angle distribution functions are reported in Fig. 8. By decreasing the system size from 4096- to 1728-atom, one obtains essentially the same results. The NN and DFT data of the small 216-atom cell are averaged over the 10 independent models. The properties averaged over the 10 NN 216-atom are close to those of the larger 4096-atom NN model. However, in the small cells we observed fluctuations in the structural properties within the 10 independent models both for NN and DFT simulations, as shown in Figs. 15–20 in the Appendix. The fluctuations are slightly larger for the NN models than for the DFT ones.

The agreement between NN and DFT data is overall very good. The largest discrepancy is on the height of the first peak of the Ge-Ge pair correlation function. Another discrepancy with the DFT results is the presence of a small peak at around 60° in the NN angle distribution function due to a very small fraction of three membered rings (see below). The same discrepancy is present in the NN angle distribution function of the liquid (cf. Fig. 5). Following our previous works,[6] we quantified the fraction of Ge atoms in a tetrahedral geometry by computing the local order parameter $q = 1 - \frac{3}{8}\sum_{i>k}(\frac{1}{3} + \cos\theta_{ijk})^2$ where the sum runs over the pairs of atoms bonded to a central atom j. $q = 1$ for the ideal tetrahedral geometry, $q = 0$ for the six-coordinated octahedral site, and $q = 5/8$ for a four-coordinated defective octahedral site. The distribution of the local order parameter q for Ge atoms is reported in Fig. 9 for different coordination numbers. The q distribution for four-coordinated Ge is bimodal with peaks corresponding to defective octahedra and tetrahedra. In contrast, the q distribution for Te does not show any signature of the tetrahedral geometry (cf. Fig. 9). We estimated the fraction of tetrahedral Ge atoms by integrating the q distribution of four-coordinated Ge from 0.8 to 1. This procedure was demonstrated to provide reliable values for the fraction of tetrahedral Ge from the analysis of the Wannier functions that allow a direct identification of the tetrahedral geometry in terms of the electronic structure.[42,53] In fact, Ge in tetrahedral sites has four bonding sp^3-like Wannier functions, while Ge in defective octahedra has three p-like bonding Wannier functions and one s-like lone pair. The fraction of tetrahedral Ge atoms for all the ten 216-atom NN models, for the large 4096-atom model, and the DFT result average over ten 216-atom models are compared in Fig. 10. The average values of the small 216-atom DFT and NN models are both very close to the value for the large 4096-atom NN model (24%) and also for an intermediate 1728-atom model (22%).

Turning now to the medium-range order, we report in Fig. 11 the distribution of ring lengths computed according to Ref. 54 for the large and small NN models and for the small DFT models. The amorphous phases of GeTe and GST have been shown to display a large concentration of nanocavities.[8] The distribution of the volume of nanocavities computed according to the definition of Ref. 55 and the algorithm of Refs. 56 and 57 is compared in Fig. 12 for the

TABLE V. Average coordination number for different pairs of atoms computed from the partial pair correlation functions of amorphous GeTe from NN molecular dynamics simulations at 300 K with a 4096- and a 216-atom cell, compared with results from DFT simulations at the same temperature of 216-atom cells. The interatomic distance thresholds defined in Fig. 6 are used.

	With Ge			With Te			Total		
	DFT	NN_{216}	NN_{4096}	DFT	NN_{216}	NN_{4096}	DFT	NN_{216}	NN_{4096}
Ge	0.76	0.78	0.88	3.28	3.31	3.22	4.03	4.09	4.10
Te	3.28	3.31	3.22	0.02	0.04	0.05	3.30	3.35	3.27

NN and DFT models. The same scheme for the calculation of nanocavities was applied in our previous works on different phase change materials.[41] These comparisons show that the agreement between NN and DFT results is very good for the medium-range order as well.

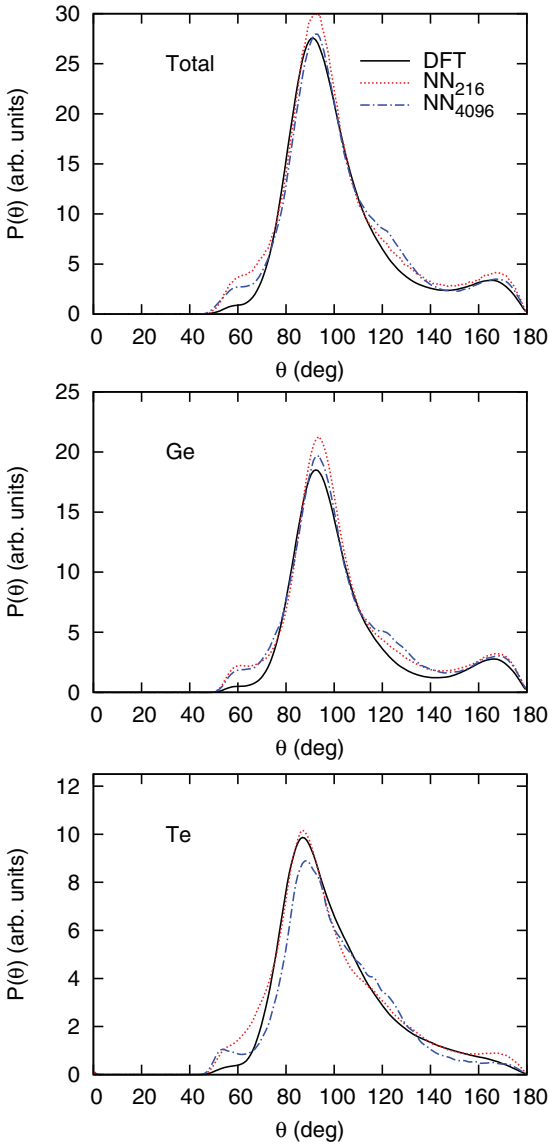

FIG. 8. (Color online) Total and partial angle distribution functions of amorphous GeTe from a NN molecular dynamics simulation at 300 K with a 4096- and 216-atom cell, compared with results from DFT simulation at the same temperature of 216-atom cells. Partial distributions refer to X-Ge-Y and X-Te-Y triplets (X,Y = Ge or Te).

We also optimized the density of the amorphous model at zero temperature by interpolating the energy-volume points with a Murnaghan equation of state. We obtained an equilibrium density of 0.03351 atoms/Å^{-3} to be compared with the value of 0.03156 atoms/Å^{-3} resulting from the DFT equation of state of a 216-atom cell with the BZ integration restricted to the Γ point.[18] The experimental equilibrium density[52] of a-GeTe is 0.03327 atoms/Å^{-3}. The NN and DFT bulk moduli of a-GeTe are 17 and 14 GPa, respectively.

Concerning the vibrational properties, the phonon density of states of amorphous GeTe from NN and DFT simulations are compared in Fig. 13. Phonon frequencies are computed by diagonalizing the dynamical matrix obtained in turn from the variation of atomic forces due to finite atomic displacements 0.02 Å large. Only phonons with the periodicity of our supercells (Γ-point phonons) were considered. *Ab initio* phonons are computed in a single 216-atom cell,[18] while NN phonons are obtained from either the 4096-atom cell or averaged over ten 216-atom models. Projections on the different type of atoms (Te, Ge in tetrahedral and defective octahedral geometries) are also shown.

In an amorphous material, phonons display localization properties, which depend on frequency. To address this issue and following our previous DFT works,[18] we computed the inverse participation ratio (IPR) of the jth vibrational mode defined as

$$\mathrm{IPR} = \frac{\sum_\kappa \left| \frac{\mathbf{e}(j,\kappa)}{\sqrt{M_\kappa}} \right|^4}{\left(\sum_\kappa \frac{|\mathbf{e}(j,\kappa)|^2}{M_\kappa} \right)^2}. \quad (1)$$

Here, $\mathbf{e}(j,\kappa)$ are phonon eigenvectors and the sum over κ runs over the N atoms in the unit cell with masses M_κ. According to this definition, the value of IPR varies from $1/N$ for a completely delocalized phonon, to one for a mode completely localized on a single atom. The values of IPR for the NN and DFT models of a-GeTe are reported in Fig. 14. The NN potential reproduces the strong localization on tetrahedra of phonons above 200 cm^{-1}. The overall shape and frequency range of the phonon DOS is reasonably reproduced by the NN potential. A discrepancy is present in the relative height of the two main structures at 50 and 150 cm^{-1}, which, however, might be partially due to the still small size of the 216-atom cell. The size of the fluctuations in the DOS among the 216-atom NN models can be appreciated in Fig. 21 in the Appendix. The total DOS averaged over the 10 models is, however, close to that of the larger 4096-atom model, although differences in the projected DOS are still sizable.

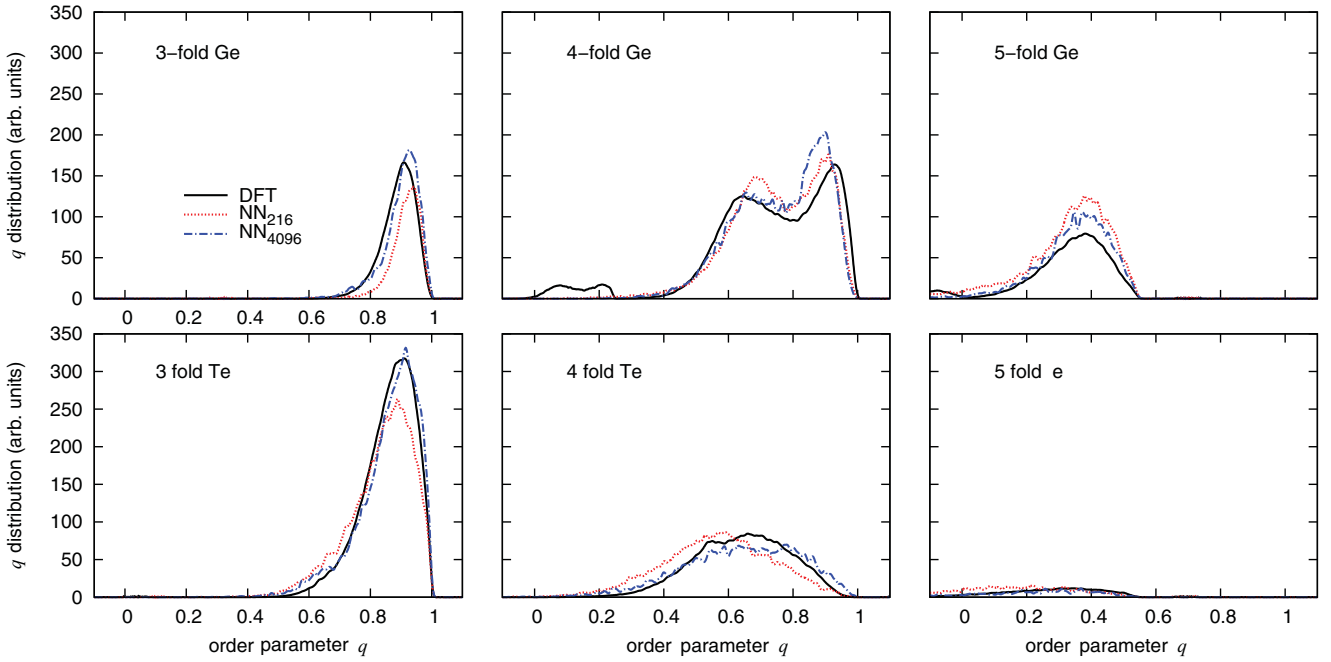

FIG. 9. (Color online) Order parameter q for tetrahedricity (see text) for threefold-, fourfold-, and fivefold-coordinated Ge and Te atoms in amorphous GeTe from NN molecular dynamics simulations at 300 K with a 4096- and 216-atom cell, compared with results from a DFT simulation at the same temperature and 216-atom cells.

IV. CONCLUSIONS

In summary, a NN potential for the phase change material GeTe has been created and tested to reproduce the properties of crystalline, liquid, and amorphous phases. The NN potential has been validated by comparing the results on structural and dynamical properties of the bulk phases of GeTe with our previous data from DFT calculations. By means of NN simulations, we have been able to study the dependence of the structural properties of a-GeTe on quenching time and system size. Actually, no sizable changes are observed in the structural properties of the large 4096-atom cell by increasing the quenching time from 100 to 300 ps from the melting temperature to 300 K. On the other hand, we observed sizable fluctuations in structural properties among 10 independent 216-atom models of a-GeTe all quenched in 100 ps both in NN and DFT simulations. However, averaging over 10 models is enough to obtain results very close to those of the large 4096-atom cell. The NN potential developed here for the GeTe stoichiometric composition can be used also for $Ge_{1-x}Te_{1+x}$ alloys with small x. However, the potential is not yet transferable to strongly off-stoichiometric composition such as the eutectic alloy $Ge_{0.15}Te_{0.85}$ because it is unable to reproduce accurately the interaction between long Te-Te chains as we explicitly checked by means of DFT simulations (no Te-Te chains but few dimers are present in $Ge_{0.5}Te_{0.5}$). The transferability of the NN potential can be systematically extended to the whole binary phase diagram of the Ge-Te compound by including new DFT configurations

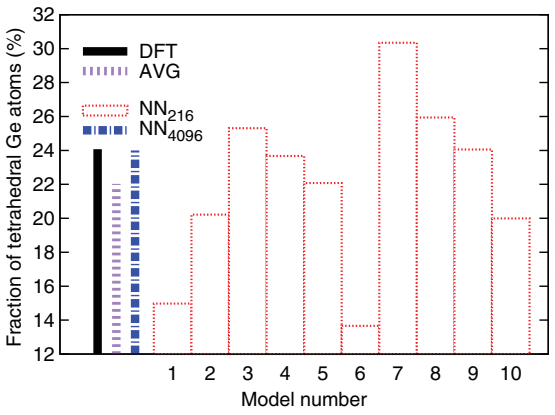

FIG. 10. (Color online) Fraction of tetrahedral Ge atoms in amorphous GeTe from 10 statistically independent 216-atom models generated with the NN potential, compared with results averaged over 10 DFT 216-atom models. The average (AVG) over the 10 NN models and from the 4096-atom model are also reported.

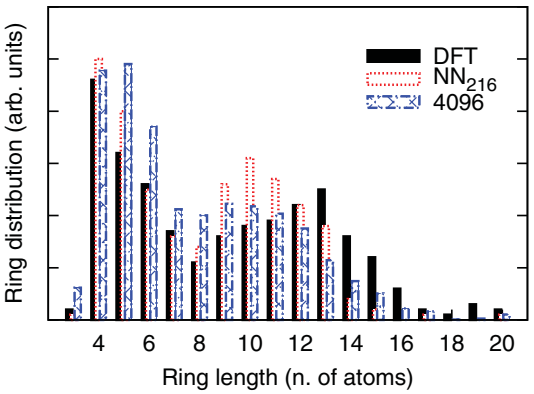

FIG. 11. (Color online) Distribution of ring lengths in the 4096- and 216-atom NN models and in the DFT 216-atom models.

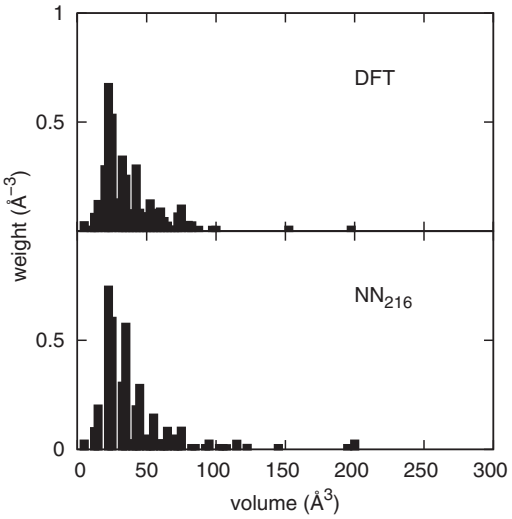

FIG. 12. Distribution of the volume of cavities in the 216-atom NN and DFT models.

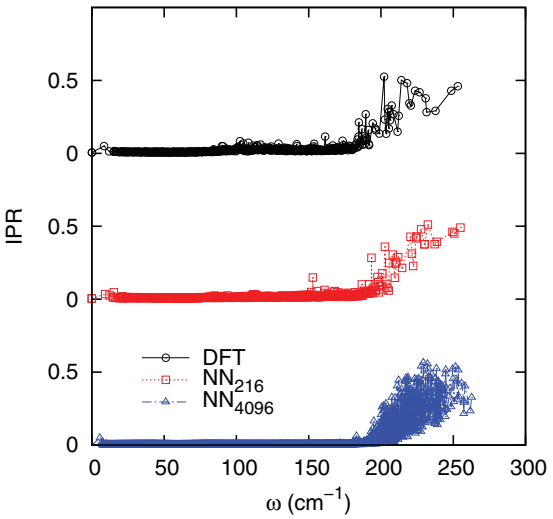

FIG. 14. (Color online) Inverse participation ratio of phonons in *a*-GeTe from the 4096-atom model and a single 216-atom NN and DFT model (Ref. 18).

in the database. The simulations with the NN potential are still sizably more expensive than simulations with classical force fields but do provide a huge speed up with respect to DFT simulations. The computational load is 1.5 min/ps on a 256 cores of Cray XT5 for the 4096-atom cell, which is five to six orders of magnitude faster than a standard Born-Oppheneimer DFT simulation with the CP2K code or at least four orders of magnitude faster than simulations with wave-function extrapolations[59] either with CP2K (Refs. 38 and 60) or with the plane-wave CPMD code.[58]

The development of a classical potential with close to DFT accuracy represents a breakthrough in the simulation of phase change materials, as it will allow addressing several key issues on the properties of this class of materials that are presently beyond the reach of DFT simulations. The study of thermal conductivity in the amorphous phase,[61] the dynamics of homogeneous and heterogeneous crystallization, and the properties of the liquid phase at high temperature[62] and in supercooled regime are few examples of useful follow-on developments of this work, which promises to improve our microscopic understanding of the operation of phase change memories.

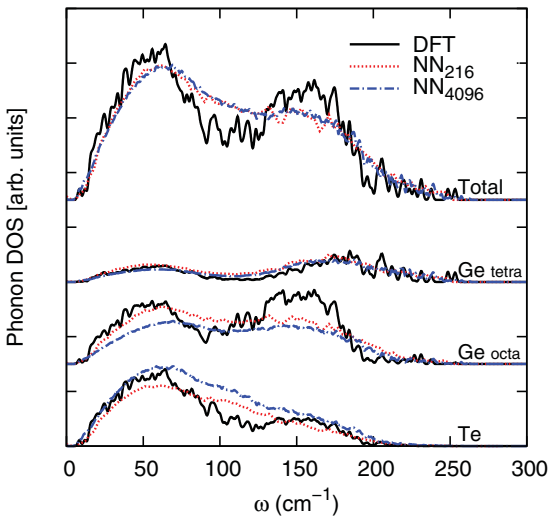

FIG. 13. (Color online) Phonon density of states of amorphous GeTe from 4096- and 216-atom NN models. Results for a single 216-atom DFT model (Ref. 18) are also reported. Only phonons at the supercell Γ point are considered. Projections of the DOS on the different atomic species (Te atoms and Ge atoms in tetrahedral and defective octahedral geometries) are also shown.

ACKNOWLEDGMENTS

This work has been partially supported by Regione Lombardia and CILEA Consortium through a LISA Initiative (Laboratory for Interdisciplinary Advanced Simulation) 2011 grant, by the Cariplo Foundation through project Monads, and by MURST through the program PRIN08. We thankfully acknowledge computational resources by DEISA Consortium under projects NETPHASE, by CSCS (Manno, Switzerland), and by the ISCRA Initiative at Cineca. J.B. thanks the DFG for financial support (Emmy Noether program).

APPENDIX

To assess the size of the fluctuations in the structural properties in a small cell, we here report the properties of *a*-GeTe for 10 independent 216-atom models generated by quenching from the melt in DFT and NN simulations. The partial and total pair correlation functions, angle distribution functions, and distribution of the coordination numbers are reported in Figs. 16, 18, and 20 and 15, 17, and 19 for NN and DFT models, respectively. Comparison with previous DFT data from Ref. 9 is also shown in Fig. 15. Phonon density of states of the ten 216-atom models are reported in Fig. 21.

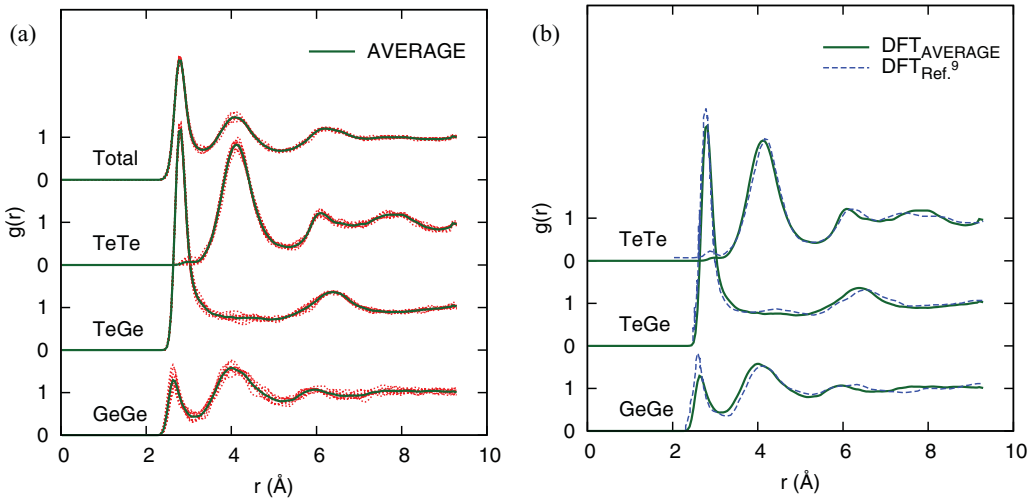

FIG. 15. (Color online) (a) Total and partial pair correlation functions of amorphous GeTe from *ab initio* molecular dynamics simulations at 300 K of 10 independent 216-atom models. (b) Partial pair correlation functions average over the ten 216-atom models compared with previous DFT results with the same cell size and the same PBE functional from Ref. 9.

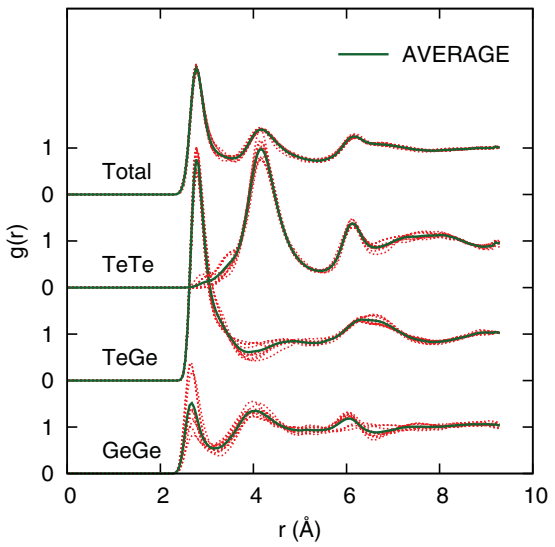

FIG. 16. (Color online) Total and partial pair correlation functions of amorphous GeTe from NN molecular dynamics simulations at 300 K of 10 independent 216-atom models. Average values are also reported.

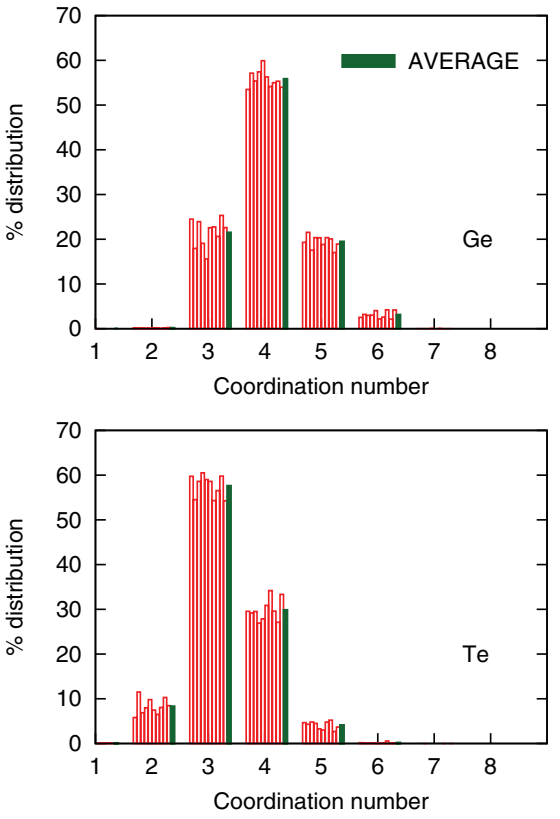

FIG. 17. (Color online) Distribution of coordination numbers of Ge and Te atoms of amorphous GeTe from DFT molecular dynamics simulations at 300 K of 10 independent 216-atom models. Average values are also reported.

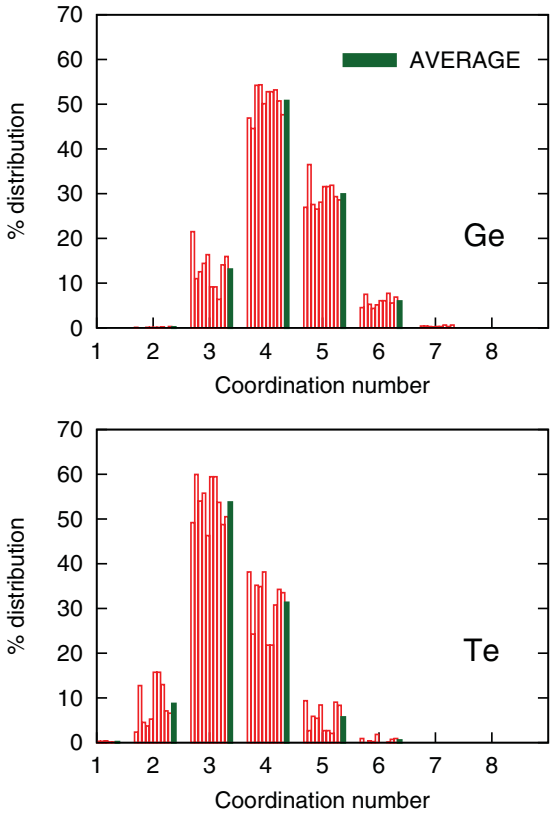

FIG. 18. (Color online) Distribution of coordination numbers of Ge and Te atoms of amorphous GeTe from NN molecular dynamics simulations at 300 K of 10 independent 216-atom models. Average values are also reported.

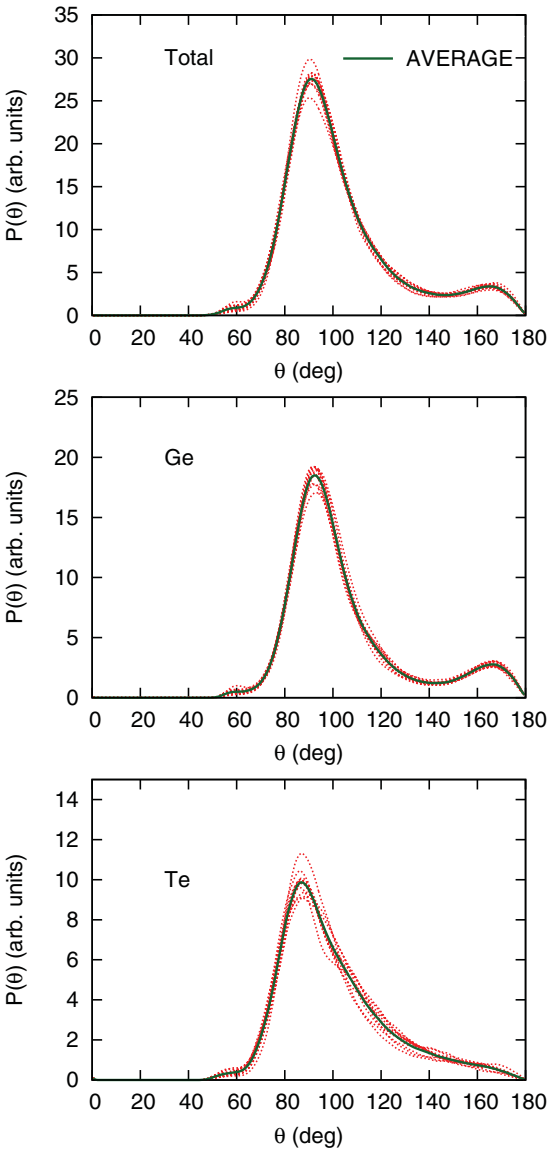

FIG. 19. (Color online) Total and partial angle distribution functions of amorphous GeTe from DFT molecular dynamics simulations at 300 K of 10 independent 216-atom models. Average values are also reported. Partial distributions refer to X-Ge-Y and X-Te-Y triplets (X,Y = Ge or Te).

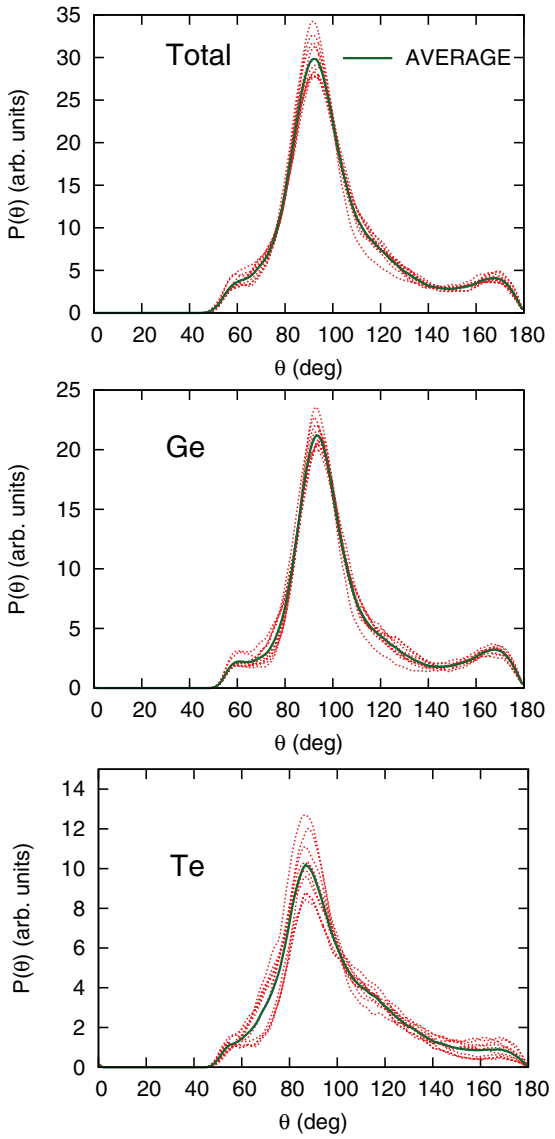

FIG. 20. (Color online) Total and partial angle distribution functions of amorphous GeTe from NN molecular dynamics simulations at 300 K of 10 independent 216-atom models. Average values are also reported. Partial distributions refer to X-Ge-Y and X-Te-Y triplets (X,Y = Ge or Te).

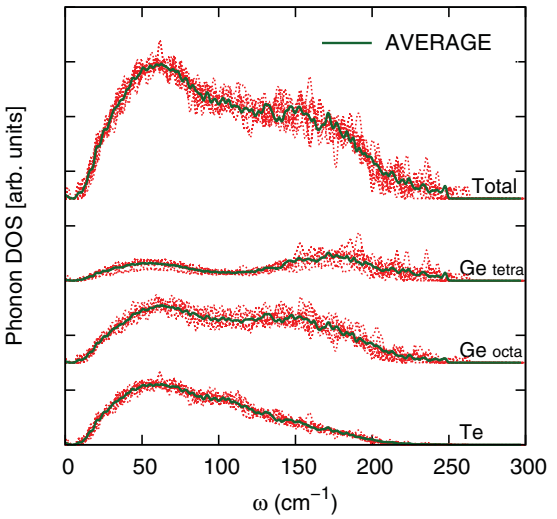

FIG. 21. (Color online) Phonon densities of states and projections on the different atomic species of 10 independent 216-atom NN models. The averaged DOS is also shown.

*Current address: Institute of Theoretical Physics, École Polytechnique Fédérale de Lausanne (EPFL), CH-1015 Lausanne, Switzerland.
†marco.bernasconi@unimib.it

[1]M. Wuttig and N. Yamada, Nat. Mater. **6**, 824 (2007).
[2]A. Pirovano, A. L. Lacaita, A. Benvenuti, F. Pellizzer, and R. Bez, IEEE Trans. Electron Devices **51**, 452 (2004).
[3]A. L. Lacaita and D. J. Wouters, Phys. Status Solidi A **205**, 2281 (2008).
[4]D. Lencer, M. Salinga, and M. Wuttig, Adv. Mater. **23**, 2030 (2011).
[5]S. Raoux, W. Welnic, and D. Ielmini, Chem. Rev. **110**, 240 (2010).
[6]S. Caravati, M. Bernasconi, T. D. Kühne, M. Krack, and M. Parrinello, Appl. Phys. Lett. **91**, 171906 (2007).
[7]S. Caravati, M. Bernasconi, T. D. Kühne, M. Krack, and M. Parrinello, J. Phys.: Condens. Matter **21**, 255501 (2009); **21**, 499803(E) (2009); **22**, 399801 (2010).
[8]J. Akola and R. O. Jones, Phys. Rev. B **76**, 235201 (2007).
[9]J. Akola and R. O. Jones, Phys. Rev. Lett. **100**, 205502 (2008).
[10]J. Behler and M. Parrinello, Phys. Rev. Lett. **98**, 146401 (2007).
[11]J. Behler, R. Martoňák, D. Donadio, and M. Parrinello, Phys. Rev. Lett. **100**, 185501 (2008).

[12]J. Behler, R. Martoňák, D. Donadio, and M. Parrinello, Phys. Status Solidi B **245**, 2618 (2008).
[13]R. Z. Khaliullin, H. Eshet, T. D. Kühne, J. Behler, and M. Parrinello, Phys. Rev. B **81**, 100103 (2010).
[14]R. Z. Khaliullin, H. Eshet, T. D. Kühne, J. Behler, and M. Parrinello, Nat. Mater. **10**, 693 (2011).
[15]H. Eshet, R. Z. Khaliullin, T. D. Kühne, J. Behler, and M. Parrinello, Phys. Rev. B **81**, 184107 (2010).
[16]N. Artrith, T. Morawietz, and J. Behler, Phys. Rev. B **83**, 153101 (2011).
[17]N. Artrith and J. Behler, Phys. Rev. B **85**, 045439 (2012).
[18]R. Mazzarello, S. Caravati, S. Angioletti-Uberti, M. Bernasconi, and M. Parrinello, Phys. Rev. Lett. **104**, 085503 (2010); **107**, 039902(E) (2011).
[19]C. M. Bishop, *Neural Networks for Pattern Recognition* (Oxford University Press, Oxford, UK, 1995).
[20]C. M. Handley and P. L. A. Popelier, J. Phys. Chem. A **114**, 3371 (2010).
[21]J. Behler, Phys. Chem. Chem. Phys. **13**, 17930 (2011).
[22]K. Hornik, M. Stinchcombe, and H. White, Neural Networks **2**, 359 (1989).
[23]G. Cybenko, Math. Control Signals Syst. **2**, 303 (1989).
[24]H. Gassner, M. Probst, A. Lauenstein, and K. Hermansson, J. Phys. Chem. A **102**, 4596 (1998).
[25]D. F. R. Brown, M. N. Gibbs, and D. C. Clary, J. Chem. Phys. **105**, 7597 (1996).
[26]L. M. Raff, M. Malshe, M. Hagan, D. I. Doughan, M. G. Rockley, and R. Komanduri, J. Chem. Phys. **122**, 084104 (2005).
[27]S. Manzhos, X. Wang, R. Dawes, and T. Carrington Jr., J. Phys. Chem. A **110**, 5295 (2006).
[28]S. Houlding, S. Y. Liem, and P. L. A. Popelier, Int. J. Quantum Chem. **107**, 2817 (2007).
[29]T. B. Blank, S. D. Brown, A. W. Calhoun, and D. J. Doren, J. Chem. Phys. **103**, 4129 (1995).
[30]S. Lorenz, A. Groß, and M. Scheffler, Chem. Phys. Lett. **395**, 210 (2004).
[31]J. Ludwig and D. G. Vlachos, J. Chem. Phys. **127**, 154716 (2007).
[32]J. Behler, S. Lorenz, and K. Reuter, J. Chem. Phys. **127**, 014705 (2007).
[33]J. Behler, K. Reuter, and M. Scheffler, Phys. Rev. B **77**, 115421 (2008).
[34]C. Carbogno, J. Behler, A. Groß, and K. Reuter, Phys. Rev. Lett. **101**, 096104 (2008).
[35]J. Behler, J. Chem. Phys. **134**, 074106 (2011).
[36]T. Morawietz, V. Sharma, and J. Behler, J. Chem. Phys. **136**, 064103 (2012).
[37]R. Martoňák, A. Laio, and M. Parrinello, Phys. Rev. Lett. **90**, 075503 (2003).
[38]J. VandeVondele, M. Krack, F. Mohamed, M. Parrinello, T. Chassaing, and J. Hutter, Comput. Phys. Commun. **167**, 103 (2005); M. Krack and M. Parrinello, in *High Performance Computing in Chemistry*, edited by J. Grotendorst (NIC, Julich, 2004), Vol. 25, pp. 29–51.
[39]J. P. Perdew, K. Burke, and M. Ernzerhof, Phys. Rev. Lett. **77**, 3865 (1996).
[40]S. Goedecker, M. Teter, and J. Hutter, Phys. Rev. B **54**, 1703 (1996); M. Krack, Theor. Chem. Acc. **114**, 145 (2005).
[41]S. Caravati, M. Bernasconi, and M. Parrinello, Phys. Rev. B **81**, 014201 (2010).
[42]E. Spreafico, S. Caravati, and M. Bernasconi, Phys. Rev. B **83**, 144205 (2011).
[43]H. J. Monkhorst and J. D. Pack, Phys. Rev. B **13**, 5188 (1976).
[44]P. Giannozzi *et al*., J. Phys.: Condens. Matter **21**, 395502 (2009).
[45]RUNNER: Neural Network Code for High-Dimensional Potential-Energy Surfaces, Jörg Behler, Lehrstuhl für Theoretische Chemie, Ruhr-Universität Bochum, Germany.
[46]TINKER: Software Tools for Molecular Design, J. W. Ponder, Department of Chemistry, Washington University, Saint Louis, USA, Version 5.1.09 (2009), [http://dasher.wustl.edu/tinker/].
[47]H. J. C. Berendsen, J. P. M. Postma, W. F. van Gunsteren, A. DiNola, and J. R. Haak, J. Chem. Phys. **81**, 3684 (1984).
[48]J. Goldak, C. S. Barrett, D. Innes, and W. Youdelis, J. Chem. Phys. **44**, 3323 (1966).
[49]F. D. Murnaghan, Proc. Natl. Acad. Sci. USA **30**, 244 (1944).
[50]D. Lencer, M. Salinga, B. Grabowski, T. Hickel, J. Neugebauer, and M. Wuttig, Nat. Mater. **7**, 972 (2008).
[51]R. Shaltaf, E. Durgun, J. Y. Raty, P. Ghosez, and X. Gonze, Phys. Rev. B **78**, 205203 (2008).
[52]G. E. Ghezzi, J. Y. Raty, S. Maitrejean, A. Roule, E. Elkaim, and F. Hippert, Appl. Phys. Lett. **99**, 151906 (2011).
[53]G. C. Sosso, S. Caravati, R. Mazzarello, and M. Bernasconi, Phys. Rev. B **83**, 134201 (2011).
[54]D. S. Franzblau, Phys. Rev. B **44**, 4925 (1991).
[55]M. G. Alinchenko, A. V. Anikeenko, N. N. Medvedev, V. P. Voloshin, M. Mezei, and P. Jedlovszky, J. Phys. Chem. B **108**, 19056 (2004).
[56]N. N. Medvedev, V. P. Voloshin, V. A. Luchnikov, and M. L. Gavrilova, J. Comput. Chem. **27**, 1676 (2006).
[57][http://www.kinetics.nsc.ru/sms/].
[58]CPMD, Version 3.11, IBM Corp., 19902011, MPI für Festkörperforschung Stuttgart, [http://www.cpmd.org].
[59]J. Kolafa, J. Comput. Chem. **25**, 335 (2004).
[60]T. D. Kühne, M. Krack, F. R. Mohamed, and M. Parrinello, Phys. Rev. Lett. **98**, 066401 (2007).
[61]G. C. Sosso, D. Donadio, S. Caravati, J. Behler, and M. Bernasconi (unpublished).
[62]J. Y. Raty, V. Godlevsky, P. Ghosez, C. Bichara, J. P. Gaspard, and J. R. Chelikowsky, Phys. Rev. Lett. **85**, 1950 (2000).